

Observation of the decay $\psi(3686) \rightarrow \Lambda \bar{\Sigma}^{\pm} \pi^{\mp} + c.c.$

M. Ablikim¹, M. N. Achasov^{8,a}, X. C. Ai¹, O. Albayrak⁴, D. J. Ambrose⁴¹, F. F. An¹, Q. An⁴², J. Z. Bai¹, R. Baldini Ferroli^{19A}, Y. Ban²⁸, J. V. Bennett¹⁸, M. Bertani^{19A}, J. M. Bian⁴⁰, E. Boger^{21,b}, O. Bondarenko²², I. Boyko²¹, S. Braun³⁷, R. A. Briere⁴, H. Cai⁴⁷, X. Cai¹, O. Cakir^{36A}, A. Calcaterra^{19A}, G. F. Cao¹, S. A. Cetin^{36B}, J. F. Chang¹, G. Chelkov^{21,b}, G. Chen¹, H. S. Chen¹, J. C. Chen¹, M. L. Chen¹, S. J. Chen²⁶, X. Chen¹, X. R. Chen²³, Y. B. Chen¹, H. P. Cheng¹⁶, X. K. Chu²⁸, Y. P. Chu¹, D. Cronin-Hennessy⁴⁰, H. L. Dai¹, J. P. Dai¹, D. Dedovich²¹, Z. Y. Deng¹, A. Denig²⁰, I. Denysenko²¹, M. Destefanis^{45A,45C}, W. M. Ding³⁰, Y. Ding²⁴, C. Dong²⁷, J. Dong¹, L. Y. Dong¹, M. Y. Dong¹, S. X. Du⁴⁹, J. Fang¹, S. S. Fang¹, Y. Fang¹, L. Fava^{45B,45C}, C. Q. Feng⁴², C. D. Fu¹, J. L. Fu²⁶, O. Fuks^{21,b}, Q. Gao¹, Y. Gao³⁵, C. Geng⁴², K. Goetzen⁹, W. X. Gong¹, W. Gradl²⁰, M. Greco^{45A,45C}, M. H. Gu¹, Y. T. Gu¹¹, Y. H. Guan¹, A. Q. Guo²⁷, L. B. Guo²⁵, T. Guo²⁵, Y. P. Guo²⁷, Y. P. Guo²⁰, Y. L. Han¹, F. A. Harris³⁹, K. L. He¹, M. He¹, Z. Y. He²⁷, T. Held³, Y. K. Heng¹, Z. L. Hou¹, C. Hu²⁵, H. M. Hu¹, J. F. Hu³⁷, T. Hu¹, G. M. Huang⁵, G. S. Huang⁴², J. S. Huang¹⁴, L. Huang¹, X. T. Huang³⁰, T. Hussain⁴⁴, C. S. Ji⁴², Q. Ji¹, Q. P. Ji²⁷, X. B. Ji¹, X. L. Ji¹, L. L. Jiang¹, X. S. Jiang¹, J. B. Jiao³⁰, Z. Jiao¹⁶, D. P. Jin¹, S. Jin¹, F. F. Jing³⁵, T. Johansson⁴⁶, N. Kalantar-Nayestanaki²², X. L. Kang¹, M. Kavatsyuk²², B. Kloss²⁰, B. Kopf³, M. Kornicer³⁹, W. Kuehn³⁷, A. Kupsc⁴⁶, W. Lai¹, J. S. Lange³⁷, M. Lara¹⁸, P. Larin¹³, M. Leyhe³, C. H. Li¹, Cheng Li⁴², Cui Li⁴², D. Li¹⁷, D. M. Li⁴⁹, F. Li¹, G. Li¹, H. B. Li¹, J. C. Li¹, K. Li³⁰, K. Li¹², Lei Li¹, P. R. Li³⁸, Q. J. Li¹, T. Li³⁰, W. D. Li¹, W. G. Li¹, X. L. Li³⁰, X. N. Li¹, X. Q. Li²⁷, X. R. Li²⁹, Z. B. Li³⁴, H. Liang⁴², Y. F. Liang³², Y. T. Liang³⁷, G. R. Liao³⁵, D. X. Lin¹³, B. J. Liu¹, C. L. Liu⁴, C. X. Liu¹, F. H. Liu³¹, Fang Liu¹, Feng Liu⁹, H. B. Liu¹¹, H. H. Liu¹⁵, H. M. Liu¹, J. Liu¹, J. P. Liu⁴⁷, K. Liu³⁵, K. Y. Liu²⁴, P. L. Liu³⁰, Q. Liu³⁸, S. B. Liu⁴², X. Liu²³, Y. B. Liu²⁷, Z. A. Liu¹, Zhiqiang Liu¹, Zhiqing Liu²⁰, H. Loehner²², X. C. Lou^{1,c}, G. R. Lu¹⁴, H. J. Lu¹⁶, H. L. Lu¹, J. G. Lu¹, X. R. Lu³⁸, Y. Lu¹, Y. P. Lu¹, C. L. Luo²⁵, M. X. Luo⁴⁸, T. Luo³⁹, X. L. Luo¹, M. Lv¹, F. C. Ma²⁴, H. L. Ma¹, Q. M. Ma¹, S. Ma¹, T. Ma¹, X. Y. Ma¹, F. E. Maas¹³, M. Maggiora^{45A,45C}, Q. A. Malik⁴⁴, Y. J. Mao²⁸, Z. P. Mao¹, J. G. Messchendorp²², J. Min¹, T. J. Min¹, R. E. Mitchell¹⁸, X. H. Mo¹, H. Moeini²², C. Morales Morales¹³, K. Moriya¹⁸, N. Yu. Muchnoi^{8,a}, Y. Nefedov²¹, I. B. Nikolaev^{8,a}, Z. Ning¹, S. Nisar⁷, X. Y. Niu¹, S. L. Olsen²⁹, Q. Ouyang¹, S. Pacetti^{19B}, M. Pelizaeus³, H. P. Peng⁴², K. Peters⁹, J. L. Ping²⁵, R. G. Ping¹, R. Poling⁴⁰, E. Prencipe²⁰, M. Qi²⁶, S. Qian¹, C. F. Qiao³⁸, L. Q. Qin³⁰, X. S. Qin¹, Y. Qiu²⁸, Z. H. Qin¹, J. F. Qiu¹, K. H. Rashid⁴⁴, C. F. Redmer²⁰, M. Ripka²⁰, G. Rong¹, X. D. Ruan¹¹, A. Sarantsev^{21,d}, K. Sch02nning⁴⁶, S. Schumann²⁰, W. Shan²⁸, M. Shao⁴², C. P. Shen², X. Y. Shen¹, H. Y. Sheng¹, M. R. Shepherd¹⁸, W. M. Song¹, X. Y. Song¹, S. Spataro^{45A,45C}, B. Spruck³⁷, G. X. Sun¹, J. F. Sun¹⁴, S. S. Sun¹, Y. J. Sun⁴², Y. Z. Sun¹, Z. J. Sun¹, Z. T. Sun⁴², C. J. Tang³², X. Tang¹, I. Tapan^{36C}, E. H. Thorndike⁴¹, D. Toth⁴⁰, M. Ullrich³⁷, I. Uman^{36B}, G. S. Varner³⁹, B. Wang²⁷, D. Wang²⁸, D. Y. Wang²⁸, K. Wang¹, L. L. Wang¹, L. S. Wang¹, M. Wang³⁰, P. Wang¹, P. L. Wang¹, Q. J. Wang¹, S. G. Wang²⁸, W. Wang¹, X. F. Wang³⁵, Y. D. Wang^{19A}, Y. F. Wang¹, Y. Q. Wang²⁰, Z. Wang¹, Z. G. Wang¹, Z. H. Wang⁴², Z. Y. Wang¹, D. H. Wei¹⁰, J. B. Wei²⁸, P. Weidenkaff²⁰, S. P. Wen¹, M. Werner³⁷, U. Wiedner³, M. Wolke⁴⁶, G. G. Wu¹⁰, L. H. Wu¹, N. Wu¹, W. Wu²⁷, Z. Wu¹, L. G. Xia³⁵, Y. Xia¹⁷, D. Xiao¹, Z. J. Xiao²⁵, Y. G. Xie¹, Q. L. Xiu¹, G. F. Xu¹, L. Xu¹, Q. J. Xu¹², Q. N. Xu³⁸, X. P. Xu³³, Z. Xue¹, L. Yan⁴², W. B. Yan⁴², W. C. Yan⁴², Y. H. Yan¹⁷, H. X. Yang¹, Y. Yang⁵, Y. X. Yang¹⁰, H. Ye¹, M. Ye¹, M. H. Ye⁶, B. X. Yu¹, C. X. Yu²⁷, H. W. Yu²⁸, J. S. Yu²³, S. P. Yu³⁰, C. Z. Yuan¹, W. L. Yuan²⁶, Y. Yuan¹, A. A. Zafar⁴⁴, A. Zallo^{19A}, S. L. Zang²⁶, Y. Zeng¹⁷, B. X. Zhang¹, B. Y. Zhang¹, C. Zhang²⁶, C. B. Zhang¹⁷, C. C. Zhang¹, D. H. Zhang¹, H. H. Zhang³⁴, H. Y. Zhang¹, J. J. Zhang¹, J. L. Zhang¹, J. Q. Zhang¹, J. W. Zhang¹, J. Y. Zhang¹, J. Z. Zhang¹, S. H. Zhang¹, X. J. Zhang¹, X. Y. Zhang³⁰, Y. Zhang¹, Y. H. Zhang¹, Z. H. Zhang⁵, Z. P. Zhang⁴², Z. Y. Zhang⁴⁷, G. Zhao¹, J. W. Zhao¹, Lei Zhao⁴², Ling Zhao¹, M. G. Zhao²⁷, Q. Zhao¹, Q. W. Zhao¹, S. J. Zhao⁴⁹, T. C. Zhao¹, X. H. Zhao²⁶, Y. B. Zhao¹, Z. G. Zhao⁴², A. Zhemchugov^{21,b}, B. Zheng⁴³, J. P. Zheng¹, Y. H. Zheng³⁸, B. Zhong²⁵, L. Zhou¹, Li Zhou²⁷, X. Zhou⁴⁷, X. K. Zhou³⁸, X. R. Zhou⁴², X. Y. Zhou¹, K. Zhu¹, K. J. Zhu¹, X. L. Zhu³⁵, Y. C. Zhu⁴², Y. S. Zhu¹, Z. A. Zhu¹, J. Zhuang¹, B. S. Zou¹, J. H. Zou¹

(BESIII Collaboration)

¹ Institute of High Energy Physics, Beijing 100049, People's Republic of China

² Beihang University, Beijing 100191, People's Republic of China

³ Bochum Ruhr-University, D-44780 Bochum, Germany

⁴ Carnegie Mellon University, Pittsburgh, Pennsylvania 15213, USA

⁵ Central China Normal University, Wuhan 430079, People's Republic of China

⁶ China Center of Advanced Science and Technology, Beijing 100190, People's Republic of China

⁷ COMSATS Institute of Information Technology, Lahore, Defence Road, Off Raiwind Road, 54000 Lahore

⁸ G.I. Budker Institute of Nuclear Physics SB RAS (BINP), Novosibirsk 630090, Russia

⁹ GSI Helmholtzcentre for Heavy Ion Research GmbH, D-64291 Darmstadt, Germany

¹⁰ Guangxi Normal University, Guilin 541004, People's Republic of China

¹¹ GuangXi University, Nanning 530004, People's Republic of China

¹² Hangzhou Normal University, Hangzhou 310036, People's Republic of China

¹³ Helmholtz Institute Mainz, Johann-Joachim-Becher-Weg 45, D-55099 Mainz, Germany

¹⁴ Henan Normal University, Xinxiang 453007, People's Republic of China

¹⁵ Henan University of Science and Technology, Luoyang 471003, People's Republic of China

¹⁶ Huangshan College, Huangshan 245000, People's Republic of China

¹⁷ Hunan University, Changsha 410082, People's Republic of China

¹⁸ Indiana University, Bloomington, Indiana 47405, USA

- ¹⁹ (A)INFN Laboratori Nazionali di Frascati, I-00044, Frascati, Italy; (B)INFN and University of Perugia, I-06100, Perugia, Italy
- ²⁰ Johannes Gutenberg University of Mainz, Johann-Joachim-Becher-Weg 45, D-55099 Mainz, Germany
- ²¹ Joint Institute for Nuclear Research, 141980 Dubna, Moscow region, Russia
- ²² KVI, University of Groningen, NL-9747 AA Groningen, The Netherlands
- ²³ Lanzhou University, Lanzhou 730000, People's Republic of China
- ²⁴ Liaoning University, Shenyang 110036, People's Republic of China
- ²⁵ Nanjing Normal University, Nanjing 210023, People's Republic of China
- ²⁶ Nanjing University, Nanjing 210093, People's Republic of China
- ²⁷ Nankai University, Tianjin 300071, People's Republic of China
- ²⁸ Peking University, Beijing 100871, People's Republic of China
- ²⁹ Seoul National University, Seoul, 151-747 Korea
- ³⁰ Shandong University, Jinan 250100, People's Republic of China
- ³¹ Shanxi University, Taiyuan 030006, People's Republic of China
- ³² Sichuan University, Chengdu 610064, People's Republic of China
- ³³ Soochow University, Suzhou 215006, People's Republic of China
- ³⁴ Sun Yat-Sen University, Guangzhou 510275, People's Republic of China
- ³⁵ Tsinghua University, Beijing 100084, People's Republic of China
- ³⁶ (A)Ankara University, Dogol Caddesi, 06100 Tandogan, Ankara, Turkey; (B)Dogus University, 34722 Istanbul, Turkey; (C)Uludag University, 16059 Bursa, Turkey
- ³⁷ Universitaet Giessen, D-35392 Giessen, Germany
- ³⁸ University of Chinese Academy of Sciences, Beijing 100049, People's Republic of China
- ³⁹ University of Hawaii, Honolulu, Hawaii 96822, USA
- ⁴⁰ University of Minnesota, Minneapolis, Minnesota 55455, USA
- ⁴¹ University of Rochester, Rochester, New York 14627, USA
- ⁴² University of Science and Technology of China, Hefei 230026, People's Republic of China
- ⁴³ University of South China, Hengyang 421001, People's Republic of China
- ⁴⁴ University of the Punjab, Lahore-54590, Pakistan
- ⁴⁵ (A)University of Turin, I-10125, Turin, Italy; (B)University of Eastern Piedmont, I-15121, Alessandria, Italy; (C)INFN, I-10125, Turin, Italy
- ⁴⁶ Uppsala University, Box 516, SE-75120 Uppsala
- ⁴⁷ Wuhan University, Wuhan 430072, People's Republic of China
- ⁴⁸ Zhejiang University, Hangzhou 310027, People's Republic of China
- ⁴⁹ Zhengzhou University, Zhengzhou 450001, People's Republic of China
- ^a Also at the Novosibirsk State University, Novosibirsk, 630090, Russia
- ^b Also at the Moscow Institute of Physics and Technology, Moscow 141700, Russia
- ^c Also at University of Texas at Dallas, Richardson, Texas 75083, USA
- ^d Also at the PNPI, Gatchina 188300, Russia

Using a sample of 1.06×10^8 $\psi(3686)$ events collected with the BESIII detector, we present the first observation of the decays of $\psi(3686) \rightarrow \Lambda \bar{\Sigma}^+ \pi^- + c.c.$ and $\psi(3686) \rightarrow \Lambda \bar{\Sigma}^- \pi^+ + c.c.$. The branching fractions are measured to be $\mathcal{B}(\psi(3686) \rightarrow \Lambda \bar{\Sigma}^+ \pi^- + c.c.) = (1.40 \pm 0.03 \pm 0.13) \times 10^{-4}$ and $\mathcal{B}(\psi(3686) \rightarrow \Lambda \bar{\Sigma}^- \pi^+ + c.c.) = (1.54 \pm 0.04 \pm 0.13) \times 10^{-4}$, where the first errors are statistical and the second ones systematic.

PACS numbers: 13.25.Gv, 13.20.Gd, 14.40.Pq

I. INTRODUCTION

Charmonium decays provide an ideal laboratory where our understanding of nonperturbative Quantum Chromodynamics (QCD) and its interplay with perturbative QCD can be tested [1]. Perturbative QCD [2, 3] predicts that the partial widths for J/ψ and $\psi(3686)$ decays into an exclusive hadronic state h are proportional to the squares of the $c\bar{c}$ wave-function overlap at zero quark separation, which are well determined from the leptonic widths. Since the strong coupling constant, α_s , is not very different at the J/ψ and $\psi(3686)$ masses, it is expected that the J/ψ and $\psi(3686)$ branching fractions of

any exclusive hadronic state h are related by

$$Q_h = \frac{\mathcal{B}(\psi(3686) \rightarrow h)}{\mathcal{B}(J/\psi \rightarrow h)} \cong \frac{\mathcal{B}(\psi(3686) \rightarrow e^+e^-)}{\mathcal{B}(J/\psi \rightarrow e^+e^-)} \cong 12\%.$$

This relation defines the "12% rule", which works reasonably well for many specific decay modes. A large violation of this rule was observed by later experiments [4–6], particularly in $\rho\pi$ decay. Recent reviews [7, 8] of relevant theories and experiments conclude that current theoretical explanations are unsatisfactory. Clearly, more experimental results are desirable.

The study of baryon spectroscopy plays an important role in the development of the quark model and in the

understanding of QCD [9]-[11]. However, our knowledge on baryon spectroscopy is limited; in particular the number of observed baryons is significantly smaller than what is expected from the quark model. For a recent review of baryon spectroscopy, see Ref. [12].

Three body charmonium decays of J/ψ and $\psi(3686)$ decays, provide a complementary approach to study the internal structure of light baryons with respect to the traditional pion (kaon) scattering experiments. Using 58 million J/ψ events, the BESII Collaboration reported the observation of a new N^* resonance [13], denoted as $N(2065)$, in $J/\psi \rightarrow p\bar{n}\pi^- + c.c.$, which was subsequently confirmed in $J/\psi \rightarrow p\bar{p}\pi^0$ [14]. More recently, with 106 million $\psi(3686)$ events, two new structures, $N(2300)$ and $N(2570)$, were observed at the BESIII experiment in $\psi(3686) \rightarrow p\bar{p}\pi^0$ decay [15] [16]. Not only excited nucleons, but also baryons with one strange quark (eg. Λ^* and Σ^*) can be studied in J/ψ and $\psi(3686)$ decays.

In this paper, we study $\psi(3686) \rightarrow \Lambda\bar{\Sigma}^+\pi^- + c.c.$ and $\psi(3686) \rightarrow \Lambda\bar{\Sigma}^-\pi^+ + c.c.$, and measure the corresponding branching fractions for the first time using 1.06×10^8 $\psi(3686)$ events collected with the Beijing Spectrometer (BESIII) detector. Further, the branching fraction of $\psi(3686) \rightarrow \Lambda\bar{\Sigma}^-\pi^+$ and that from J/ψ decay are used to test the “12% rule” [2, 3]. Peaks are observed around 1.5 GeV/ c^2 to 1.7 GeV/ c^2 in the $\bar{\Sigma}^+\pi^-$ and $\Lambda\pi^-$ mass spectra, which are indicative of Λ^* and Σ^* states, respectively.

II. DETECTOR AND MONTE CARLO SIMULATION

The Beijing Electron Positron Collider (BEPCII) [17] is a double-ring e^+e^- collider designed to provide a peak luminosity of $10^{33} \text{ cm}^{-2}\text{s}^{-1}$ at a center of mass energy of 3.77 GeV. The BESIII [17] detector has a geometrical acceptance of 93% of 4π and has four main components: (1) A small-cell, helium-based (40% He, 60% C_3H_8) main drift chamber (MDC) with 43 layers providing an average single-hit resolution of 135 μm , and charged-particle momentum resolution in a 1 T magnetic field of 0.5% at 1 GeV/ c . (2) An electromagnetic calorimeter (EMC) consisting of 6240 CsI(Tl) crystals in a cylindrical structure (barrel) and two endcaps. For 1 GeV photons, the energy resolution is 2.5% (5%) and the position resolution is 6 mm (9 mm) in the barrel (endcaps). (3) A time-of-flight system (TOF) consisting of 5-cm-thick plastic scintillators, with 176 detectors of 2.4 m length in two layers in the barrel and 96 fan-shaped detectors in the endcaps. The barrel (endcaps) time resolution of 80 ps (110 ps) provides 2σ K/π separation for momenta up to ~ 1 GeV/ c . (4) The muon system consisting of 1000 m^2 of resistive plate chambers in 9 barrel and 8 endcap layers and providing a position resolution of 2 cm.

The optimization of the event selection and the estima-

tion of backgrounds are performed through Monte Carlo (MC) simulations. The GEANT4 [18] based simulation software BOOST [19] includes the geometry and material description of the BESIII spectrometer and the detector response and digitization models, as well as the tracking of the detector running conditions and performance. The production of the $\psi(3686)$ resonance is simulated by the MC event generator KKMC [20, 21], while the decays are generated by EVTGEN [22] for known decay modes with branching fractions being set to world average values [9], and by LUNDCHARM [23] for the remaining unknown decays.

III. EVENT SELECTION

In this analysis, the charge-conjugate reaction is always implied unless explicitly mentioned. The $\bar{\Sigma}^-$ is reconstructed in its $\bar{p}\pi^0$ and $\bar{n}\pi^-$ decay modes, and $\bar{\Sigma}^+$, Λ and π^0 are reconstructed in $\bar{\Sigma}^+ \rightarrow \bar{n}\pi^+$, $\Lambda \rightarrow p\pi^-$ and $\pi^0 \rightarrow \gamma\gamma$. The possible final states of $\psi(3686) \rightarrow \Lambda\bar{\Sigma}^+\pi^-$ and $\psi(3686) \rightarrow \Lambda\bar{\Sigma}^-\pi^+$ are then $p\pi^-\pi^-\pi^+\bar{n}$ and $\gamma\gamma\bar{p}\bar{p}\pi^-\pi^+$. The following common selection criteria, including charged track selection, particle identification and Λ reconstruction, are used to select candidate events.

Candidate events must have four charged tracks with zero net charge. Tracks, reconstructed from the MDC hits, must have a polar angle θ in the range $|\cos\theta| < 0.93$ and pass within 20 cm of the interaction point in the beam direction and within 10 cm in the plane perpendicular to the beam. The pion produced directly from $\psi(3686)$ decays must have its point of closest approach to the beam line within 20 cm of the interaction point along the beam direction and within 2.0 cm in the plane perpendicular to the beam. In order to suppress background events from $\psi(3686) \rightarrow K_S^0\bar{n}\Lambda$, the point of closest approach in the plane perpendicular to the beam is required to be within 0.5 cm in the cases of $\bar{\Sigma}^- \rightarrow \bar{n}\pi^- + c.c.$ and $\bar{\Sigma}^+ \rightarrow \bar{n}\pi^+ + c.c.$

For each charged track, both TOF and dE/dx information are combined to form Particle IDentification (PID) confidence levels for the π , K , and p hypotheses ($Prob(i)$, $i = \pi, K, p$). A charged track is identified as a pion or proton if its $Prob$ is larger than those for any other assignment. For all four channels with a neutron (or anti-neutron), only one charged track is required to be identified as a proton or anti-proton, and the other charged tracks are assigned as pions. In order to suppress background events from $\psi(3686) \rightarrow \pi^0\pi^0 J/\psi$ with $J/\psi \rightarrow \Lambda\Lambda$, the candidate pion should not be identified as an anti-proton in the case of $\bar{\Sigma}^- \rightarrow \bar{n}\pi^- + c.c.$. For $\bar{\Sigma}^- \rightarrow \bar{p}\pi^0 + c.c.$, at least one of the charged tracks should be identified as a proton or an anti-proton.

To reconstruct the decay $\Lambda \rightarrow p\pi^-$, a vertex fitting algorithm is applied to all combinations of $p\pi^-$ pairs. If

more than one $p\pi^-$ combination satisfies the vertex fitting requirement, the pair with the mass closest to $M(\Lambda)$ is chosen, where $M(\Lambda)$ is the nominal mass of Λ [9].

$$\text{A. } \psi(3686) \rightarrow \Lambda \bar{\Sigma}^- \pi^+ \rightarrow p \bar{p} \pi^+ \pi^- \gamma \gamma$$

Events selected with the above selection criteria and at least two photon candidates are kept for further analysis. Photon candidates, reconstructed by clustering EMC crystal energies, must have a minimum energy of 25 MeV for the barrel ($|\cos\theta| < 0.80$) and 50 MeV for the end-cap ($0.86 < |\cos\theta| < 0.92$), must satisfy EMC cluster timing requirements to suppress electronic noise and energy deposits unrelated to the event, and be separated by at least 10° from the nearest charged track (20° if the charged track is identified as an anti-proton) to exclude energy deposits from charged particles.

Figure 1(a) shows the $p\pi^-$ mass, $M(p\pi^-)$, distribution for events that satisfy the Λ vertex finding algorithm. A clear peak at the Λ mass is observed, and a Λ mass window requirement, $1.111 \text{ GeV}/c^2 < M(p\pi^-) < 1.121 \text{ GeV}/c^2$, is applied to extract the Λ signal.

A four-constraint kinematic fit imposing momentum and energy conservation is performed under the $\gamma\gamma p\bar{p}\pi^-\pi^+$ hypothesis, and the chisquare ($\chi^2_{\gamma\gamma p\bar{p}\pi^-\pi^+}$) is required to be less than 100. For events with more than two photons, all combinations are tried, and the combination with the smallest $\chi^2_{\gamma\gamma p\bar{p}\pi^-\pi^+}$ is retained. The π^0 is clearly seen in the $\gamma\gamma$ mass, $M(\gamma\gamma)$, spectrum shown in Fig. 1(b). The $\bar{p}\pi^0$ invariant mass spectrum for events in the π^0 mass window ($0.12 \text{ GeV}/c^2 < M(\gamma\gamma) < 0.145 \text{ GeV}/c^2$) is shown in Fig. 2(a), where the $\bar{\Sigma}^-$ peak is seen.

To extract the number of $\bar{\Sigma}^-$ events, an unbinned maximum likelihood fit is applied to the $\bar{p}\pi^0$ mass spectrum with a double Gaussian function for the signal plus a second order Chebychev polynomial as the background function. The fit, shown as the solid line in Fig. 2(a), yields $458 \pm 23 \bar{\Sigma}^-$ events, while the fit to the $p\pi^0$ mass distribution gives $554 \pm 26 \Sigma^+$ events, as shown in Fig. 2(b). The non-peaking background can be well described by the events from Λ sideband. Fits of the Λ and $\bar{\Lambda}$ sideband events yield $18 \pm 5 \bar{\Sigma}^-$ and $13 \pm 5 \Sigma^+$ events.

$$\text{B. } \psi(3686) \rightarrow \Lambda \bar{\Sigma}^+ \pi^- (\Lambda \bar{\Sigma}^- \pi^+) \rightarrow p \bar{n} \pi^+ \pi^- \pi^-$$

Neutrons cannot be fully reconstructed with the EMC information. However, the distribution of mass recoiling against $p\pi^+\pi^-\pi^-$ tracks, $R(p\pi^+\pi^-\pi^-)$, for events with the recoiling mass and the π^+ mass, $M(R(p\pi^+\pi^-\pi^-)\pi^+)$, inside the $\bar{\Sigma}^+$ mass region ($1.186 < M(R(p\pi^+\pi^-\pi^-)\pi^+) < 1.208 \text{ GeV}/c^2$), shown in Fig. 3, has a significant anti-neutron peak. After requiring $|R(p\pi^+\pi^-\pi^-) - M(\bar{n})| < 0.04 \text{ GeV}/c^2$ (3σ), where $M(\bar{n})$

is the neutron mass, a one-constraint kinematic fit with the recoil mass constrained to the neutron mass is performed to improve the mass resolution, and the chisquare $\chi^2(p\pi^-\pi^-\pi^+\bar{n})$ is required to be less than 20.

Using the same method described in Section A, we perform fits to the $\bar{n}\pi^+$, $n\pi^-$, $n\pi^+$, and $\bar{n}\pi^-$ mass distributions ($M(\bar{n}\pi^+)$, $M(n\pi^-)$, $M(n\pi^+)$ and $M(\bar{n}\pi^-)$) to extract the number of $\bar{\Sigma}^+$, Σ^- , Σ^+ and $\bar{\Sigma}^-$ events and background events from the Λ sideband. Here, the n and \bar{n} momenta from the one-constraint kinematic fits above are used to determine $M(\bar{n}\pi^+)$, $M(n\pi^-)$, $M(n\pi^+)$ and $M(\bar{n}\pi^-)$. The fits are shown in Figs. 4(a) to 4(d), and the fit results are summarized in Table I.

IV. BACKGROUND STUDY

In this analysis, 106 million inclusive $\psi(3686)$ MC events are used to investigate possible backgrounds from $\psi(3686)$ decays. The results indicate that the background events mainly have an approximately flat distribution. Since the background contributions to the Σ peak are not very significant, and the branching fractions of some possible decay channels are not yet well measured, background contributions are estimated from Λ sidebands, defined as $1.1027 \text{ GeV}/c^2 < M(p\pi^-) < 1.1077 \text{ GeV}/c^2$ and $1.1237 \text{ GeV}/c^2 < M(p\pi^-) < 1.1337 \text{ GeV}/c^2$, and shown in Fig. 5(a), where $M(p\pi^-)$ is the $p\pi^-$ invariant mass. Fitting the Λ sideband events in the same way as the signal events, we obtain the numbers of background events, summarized in Table I, which will be subtracted in the calculation of the branching fractions.

To estimate the number of background events coming directly from the e^+e^- annihilation, the same analysis is performed on data taken at center-of-mass energy of 3.65 GeV, where the number of background events are also extracted by fitting the $\bar{n}\pi^+$ (or $\bar{p}\pi^0$) mass spectrum. The background events are then normalized to the $\psi(3686)$ data after taking into account the luminosities and energy-dependent cross section of the quantum electrodynamics (QED) processes,

$$N_{QED} = \frac{\mathcal{L}_{3.686}}{\mathcal{L}_{3.650}} \times \frac{3.65^2}{3.686^2} \times N_{3.65}^{fit}, \quad (1)$$

where N_{QED} is the number of background events from QED processes, $\mathcal{L}_{3.686} = 165 \text{ pb}^{-1}$ and $\mathcal{L}_{3.650} = 44 \text{ pb}^{-1}$ are the integrated luminosities for $\psi(3686)$ data [24] and 3.65 GeV data [25], and $N_{3.65}^{fit}$ is the number of selected events from continuum data.

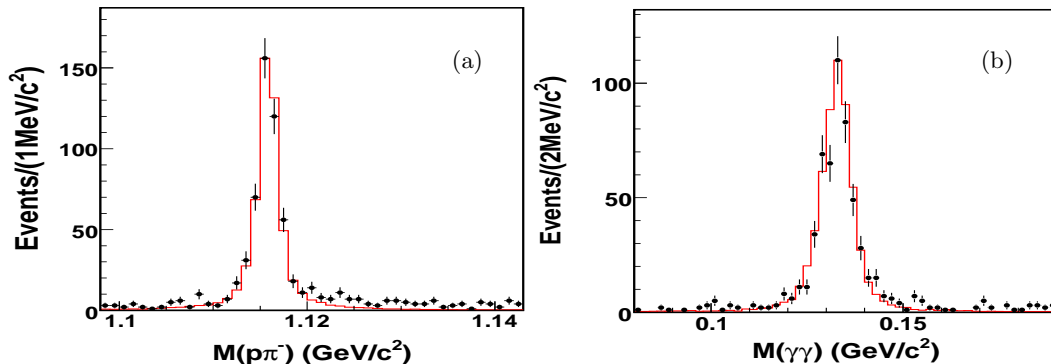


FIG. 1: The distributions of (a) $M(p\pi^-)$ and (b) $M(\gamma\gamma)$. The crosses with error bars are data, and the histograms are signal MC simulations without background included.

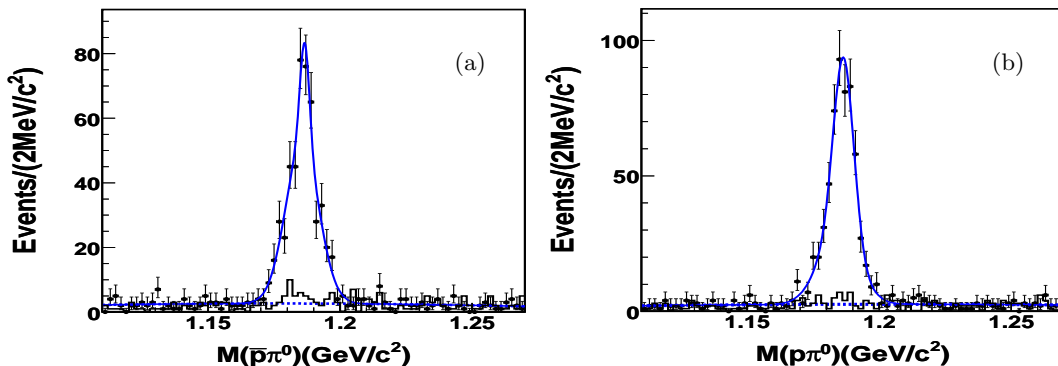


FIG. 2: The distributions of (a) $M(\bar{p}\pi^0)$ and (b) $M(p\pi^0)$. The crosses with error bars are data, the histograms are background estimated with $\Lambda(\bar{\Lambda})$ sidebands, the solid lines are the fits described in the text, and the dashed lines are the fits of background.

V. DETECTION EFFICIENCY DETERMINATION

To determine the detection efficiencies, possible intermediate states decaying into $\bar{\Sigma}\pi$ and $\Lambda\pi$ are investigated. Figure 5(b) is the Dalitz plot of selected $\psi(3686) \rightarrow \Lambda\bar{\Sigma}^+\pi^- \rightarrow p\bar{n}\pi^+\pi^-\pi^-$ candidates, where clear clusters indicate that this process is mediated by excited baryons. The two dimensional $\Lambda-\bar{\Sigma}$ sidebands, shown as the boxes in Fig. 5(a), are used to estimate the number of background events, and the background distributions, shown as shaded histograms in Figs. 6(a), 6(b) and 6(c), indicate that the structures are not from background events. The $\Lambda\pi$ and $\Sigma\pi$ invariant mass spectra, shown in Fig. 6(a) and Fig. 6(b), indicate Λ^* and Σ^* structures, eg. peaks around $1.4 \text{ GeV}/c^2$ to $1.7 \text{ GeV}/c^2$ in the invariant mass distributions of $\Lambda\pi^-$ and $\bar{\Sigma}^+\pi^-$, that clearly deviate from what is expected according to phase space. In order to determine the correct detection efficiency, a Partial Wave Analysis (PWA) is performed based on an unbinned maximum likelihood fit [13]. As shown in Fig. 6, the background contamination is small and is ignored in the PWA. Sixteen possible intermediate excited states

($\Lambda(1810)$, $\Lambda(1800)$, $\Lambda(1670)$, $\Lambda(1600)$, $\Lambda(1405)$, $\Lambda(1116)$, $\Lambda(2325)$, $\Lambda(1890)$, $\Lambda(1690)$, $\Lambda(1520)$, $\Lambda(1830)$, $\Lambda(1820)$, $\Sigma(1660)$, $\Sigma(1670)$, $\Sigma(1580)$ and $\Sigma(1385)$) with at least two stars according to the PDG [9] are included in the PWA. In the global fit, all of these resonances are described with Breit-Wigner functions, and the masses and widths are fixed to the world average [9]. A comparison of the data and global fitting results, shown in Fig. 6, indicates that the PWA results are consistent with data. A similar PWA is also performed for the decays $\psi(3686) \rightarrow \Lambda\bar{\Sigma}^-\pi^+ \rightarrow p\bar{p}\pi^+\pi^-\gamma\gamma$, and the results are also in agreement with data. Finally the MC samples of $\psi(3686) \rightarrow \Lambda\bar{\Sigma}^+\pi^-$ and $\psi(3686) \rightarrow \Lambda\bar{\Sigma}^-\pi^+$ are generated according to the PWA results, and the detection efficiencies are determined by fitting the Σ signal and Λ sideband events and presented in Table I. In the determination of the detection efficiencies, the branching fractions of the unstable intermediates (eg. Λ , $\bar{\Sigma}^+$) are included by generating all their possible decay modes in the corresponding MC samples.

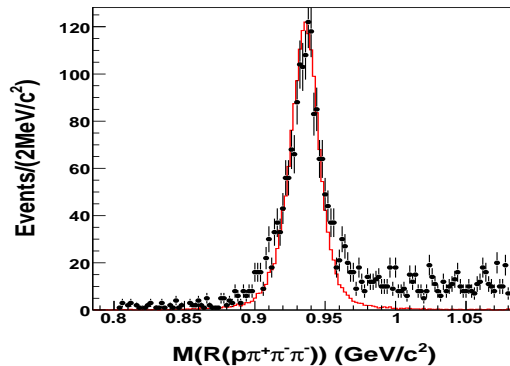


FIG. 3: The distribution of the mass recoiling against $p\pi^+\pi^-\pi^-$, where the crosses with error bars are data and the histogram the MC simulation of signal events.

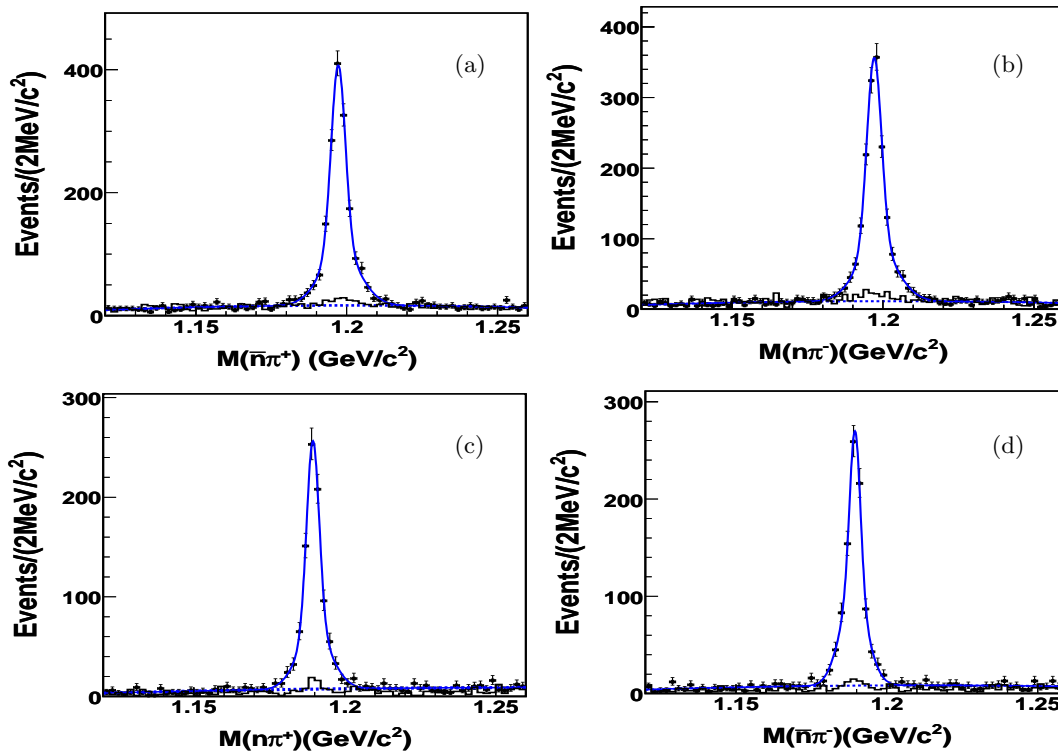


FIG. 4: The distributions of (a) $M(\bar{n}\pi^+)$, (b) $M(n\pi^-)$, (c) $M(n\pi^+)$, and (d) $M(\bar{n}\pi^-)$. The crosses with error bars are data, the histograms are background estimated with $\Lambda(\bar{\Lambda})$ sidebands, the solid lines are the fits described in the text, and the dashed lines are the fits of background.

VI. SYSTEMATIC UNCERTAINTIES

The systematic uncertainty due to the charged track detection efficiency has been studied with control samples $J/\psi \rightarrow pK^-\bar{\Lambda} + c.c.$ and $J/\psi \rightarrow \Lambda\bar{\Lambda}$ decays. The difference of the charged tracking efficiencies between data and MC simulation is 2% per track. In this analysis, there are four charged tracks in the final states, and the uncertainty is determined to be 8%.

The PID efficiency for MC simulated events agrees

with the one determined using data within 1% for each proton or anti-proton according to the study of $J/\psi \rightarrow p\bar{p}\pi^+\pi^-$ [15]. 1% is taken as the uncertainty from PID in each channel. The photon reconstruction efficiency is studied using the control sample of $J/\psi \rightarrow \rho^0\pi^0$ events, as described in [26]. The efficiency difference between data and MC simulated events is within 1% for each photon.

In order to estimate the uncertainty due to the fitting range and the background function in fitting of $\Sigma^\pm \rightarrow \bar{n}\pi^\pm$: from $[1.12 \text{ GeV}/c^2,$

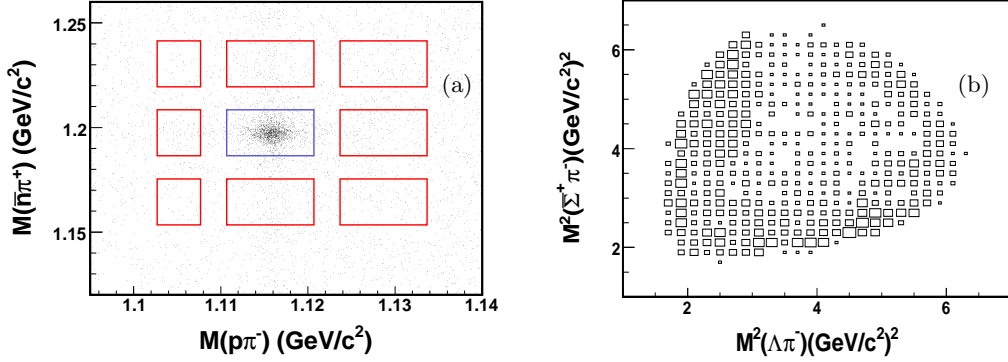


FIG. 5: (a) The scatter plot of $M(p\pi^-)$ versus $M(\bar{n}\pi^+)$, where the boxes denote the signal regions and the sideband regions for background estimation; (b) the Dalitz plot of $\psi(3686) \rightarrow \Lambda\bar{\Sigma}^+\pi^-$ candidate events.

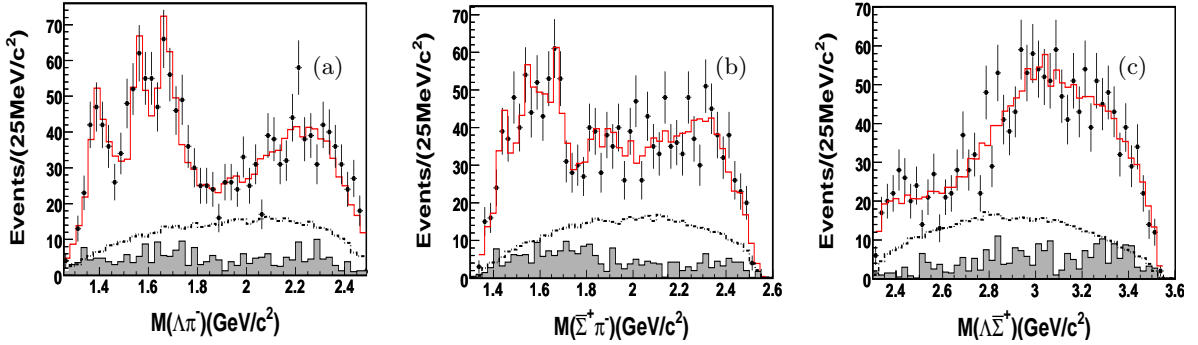


FIG. 6: Comparisons between data and PWA projections of $\psi(3686) \rightarrow \Lambda\bar{\Sigma}^+\pi^-$, (a) $M(\Lambda\pi^-)$, (b) $M(\Sigma^+\pi^-)$ and (c) $M(\Lambda\Sigma^+)$. Points with error bars are data, the solid histograms are PWA projections, the dashed histograms are phase space distributions from MC simulation, and the shaded histograms are the background contributions estimated from the $\Lambda - \bar{\Sigma}$ sidebands.

$1.26 \text{ GeV}/c^2$ to $[1.14 \text{ GeV}/c^2, 1.24 \text{ GeV}/c^2]$, $\bar{\Sigma}^- \rightarrow \bar{p}\pi^0$: from $[1.11 \text{ GeV}/c^2, 1.27 \text{ GeV}/c^2]$ to $[1.13 \text{ GeV}/c^2, 1.25 \text{ GeV}/c^2]$ have been used to perform the fitting and several polynomials (from 2nd-order polynomial to 3rd-order) have been used to describe the backgrounds. The changes of the fitting results are treated as the corresponding systematic errors.

The uncertainty associated with the 4C kinematic fit is estimated to be 1.7% using the control sample of $\psi(3686) \rightarrow \pi^+\pi^-J/\psi$, $J/\psi \rightarrow p\bar{p}\pi^0$, $\pi^0 \rightarrow \gamma\gamma$. The uncertainty associated with the 1C kinematic fit is estimated to be 2.0% using the control sample $\psi(3686) \rightarrow \pi^+\pi^-J/\psi$, $J/\psi \rightarrow p\bar{n}\pi^-$.

For the detection efficiency derived from the PWA, another MC sample is generated with only six dominant intermediate excited baryon states ($\Lambda(1116)$, $\Lambda(1520)$, $\Lambda(1670)$, $\Sigma(1385)$, $\Sigma(1580)$, $\Sigma(1670)$), and the difference of the detection efficiencies obtained from the two different MC samples is taken as the uncertainty from intermediate excited states.

The uncertainties of the branching fractions are 0.78% for $\Lambda \rightarrow p\pi$, 0.58% for $\Sigma^+ \rightarrow p\pi^0$, 0.62% for $\Sigma^+ \rightarrow n\pi^+$, 0.01% for $\Sigma^- \rightarrow n\pi^-$ and 0.04% for $\pi^0 \rightarrow \gamma\gamma$ [9]. The number of $\psi(3686)$ events is determined to be $106.41 \times$

$(1.00 \pm 0.81\%) \times 10^6$ with the inclusive hadronic events, and its uncertainty is 0.81% [25].

The sources of the systematic errors discussed above and the corresponding contributions in the error on the branching fractions are summarized in Table II. The total systematic errors are obtained by adding the contributions from all sources in quadrature.

VII. RESULTS

For the decays analyzed in this analysis, the branching fractions are obtained using the following formula:

$$\mathcal{B}(\psi(3686) \rightarrow \Lambda\bar{\Sigma}^+\pi^- (\Lambda\bar{\Sigma}^-\pi^+)) = \frac{N_{obs} - N_{sid} - N_{QED}}{N_{\psi(3686)} \times \varepsilon}, \quad (2)$$

where N_{obs} is the number of observed $\bar{\Sigma}^+$ ($\bar{\Sigma}^-$) events, N_{sid} is the number of background events estimated from Λ sidebands, N_{QED} is the number of background events from QED processes, ε is the detection efficiency obtained from the MC simulation after accounting for the branching fractions of intermediate states, and $N_{\psi(3686)}$ is the

TABLE I: The branching fractions and the values used in the calculation for each decay mode, where the first error is statistic error and the second is systematic one.

$\psi(3686) \rightarrow$	N_{obs}	N_{sid}	N_{QED}	$\varepsilon(\%)$	$\mathcal{B}(\times 10^{-5})$
$\Lambda\bar{\Sigma}^+\pi^-(\Sigma^+ \rightarrow \bar{n}\pi^+)$	1594 ± 48	43 ± 10	64 ± 16	20.25 ± 0.15	$6.91 \pm 0.25 \pm 0.65$
$\bar{\Lambda}\Sigma^-\pi^+(\Sigma^- \rightarrow n\pi^-)$	1637 ± 47	44 ± 10	54 ± 14	20.55 ± 0.15	$7.05 \pm 0.24 \pm 0.61$
$\Lambda\Sigma^-\pi^+(\Sigma^- \rightarrow \bar{n}\pi^-)$	898 ± 35	28 ± 6	25 ± 12	10.03 ± 0.11	$7.93 \pm 0.36 \pm 0.70$
$\bar{\Lambda}\Sigma^+\pi^-(\Sigma^+ \rightarrow n\pi^+)$	891 ± 35	29 ± 6	32 ± 11	10.22 ± 0.11	$7.64 \pm 0.35 \pm 0.69$
$\Lambda\Sigma^-\pi^+(\Sigma^- \rightarrow \bar{p}\pi^0)$	458 ± 23	18 ± 5	26 ± 10	5.34 ± 0.078	$7.29 \pm 0.47 \pm 0.72$
$\bar{\Lambda}\Sigma^+\pi^-(\Sigma^+ \rightarrow p\pi^0)$	554 ± 26	13 ± 5	33 ± 11	6.22 ± 0.081	$7.68 \pm 0.67 \pm 0.71$

number of $\psi(3686)$ events, which is determined from the inclusive hadronic events [25].

The resulting branching fractions are summarized in Table I, in which the first errors are statistical and the second ones systematic.

VIII. SUMMARY

Based on 106 million $\psi(3686)$ events collected with the BESIII detector, the decays $\psi(3686) \rightarrow \Lambda\bar{\Sigma}^+\pi^- + c.c.$ and $\psi(3686) \rightarrow \bar{\Lambda}\Sigma^-\pi^+ + c.c.$ are analyzed, and excited strange baryons (eg. peaks around 1.5 GeV/ c^2 to 1.7 GeV/ c^2 in the invariant mass spectra of $\bar{\Sigma}^+\pi^-$ and $\Lambda\pi^-$) are observed. The branching fractions are measured for the first time and summarized in Table I. For each decay mode, the branching fraction is in good agreement with its charge-conjugate reaction. With the approach proposed in Ref. [27], the weighted average of the measurements are determined to be

$$\begin{aligned} \mathcal{B}(\psi(3686) \rightarrow \Lambda\bar{\Sigma}^+\pi^- + c.c.) &= (1.40 \pm 0.03 \pm 0.13) \times 10^{-4}, \\ \mathcal{B}(\psi(3686) \rightarrow \bar{\Lambda}\Sigma^-\pi^+ + c.c.) &= (1.54 \pm 0.04 \pm 0.13) \times 10^{-4}, \end{aligned}$$

where the first errors are statistical and the second ones systematic.

With the branching fraction of $J/\psi \rightarrow \Lambda\bar{\Sigma}^-\pi^+$ [9], we obtain:

$$Q_{\Lambda\bar{\Sigma}^-\pi^+} = \frac{\mathcal{B}(\psi(3686) \rightarrow \Lambda\bar{\Sigma}^-\pi^+)}{\mathcal{B}(J/\psi \rightarrow \Lambda\bar{\Sigma}^-\pi^+)} = (9.3 \pm 1.2)\%, \quad (3)$$

which tests the “12% rule” for this decay.

IX. ACKNOWLEDGMENTS

The BESIII collaboration thanks the staff of BEPCII and the computing center for their hard efforts. This work is supported in part by the Ministry of Science and Technology of China under Contract No. 2009CB825200; National Natural Science Foundation of China (NSFC) under Contracts Nos. 10625524, 10805053, 10821063, 10825524, 10835001, 10935007, 11125525, 10979038, 11079030, 11005109; Joint Funds of the National Natural Science Foundation of China under Contracts Nos. 11079008, 11179007, 10979012, U1232107; the Chinese Academy of Sciences (CAS) Large-Scale Scientific Facility Program; CAS under Contracts Nos. KJCX2-YW-N29, KJCX2-YW-N45; 100 Talents Program of CAS; Istituto Nazionale di Fisica Nucleare, Italy; Ministry of Development of Turkey under Contract No. DPT2006K-120470; U. S. Department of Energy under Contracts Nos. DE-FG02-04ER41291, DE-FG02-91ER40682, DE-FG02-94ER40823; U.S. National Science Foundation; University of Groningen (RuG); the Helmholtzzentrum fuer Schwerionenforschung GmbH (GSI), Darmstadt; and WCU Program of National Research Foundation of Korea under Contract No. R32-2008-000-10155-0.

-
- [1] D. M. Asner, T. Barnes, J. M. Bian, I. I. Bigi, N. Brambilla, I. R. Boyko, V. Bytev and K. T. Chao *et al.* Int. J. Mod. Phys. A **24**, S1 (2009).
- [2] T. Appelquist *et al.*, Phys. Rev. Lett. **34**, 43 (1975).
- [3] A. De Rujula *et al.*, Phys. Rev. Lett. **34**, 46 (1975).
- [4] M. E. B. Franklin *et al.* (MARKII Collaboration), Phys. Rev. Lett. **51**, 963 (1983).
- [5] M. Ablikim *et al.* (BES Collaboration), Phys. Lett. B **614**, 37 (2005).
- [6] R. A. Briere *et al.* (CLEO Collaboration), Phys. Rev. Lett. **95**, 062001 (2005).
- [7] N. Brambilla *et al.* (Quarkonium Working Group), Eur. Phys. J. C **71**, 1534 (2011).
- [8] Q. Wang *et al.*, Phys. Rev. D **85**, 074015 (2012).
- [9] J. Beringer *et al.* (Particle Data Group), Phys. Rev. D **86**, 010001 (2012).
- [10] S. Capstick and W. Roberts *et al.* Prog. Part. Nucl. Phys. **45**, S241 (2000).
- [11] K. F. Liu and C. W. Wong, Phys. Rev. D **28**, 170 (1983).
- [12] E. Klempt and J. Richard, Rev. Mod. Phys **82**, 1095

TABLE II: Summary of systematic sources and the corresponding contributions (%).

$\psi(3686) \rightarrow$ Sources	$\Lambda\Sigma^+\pi^-$ ($\bar{\Sigma}^+ \rightarrow \bar{n}\pi^+$)	$\Lambda\Sigma^-\pi^+$ ($\Sigma^- \rightarrow \bar{n}\pi^-$)	$\Lambda\Sigma^-\pi^+$ ($\bar{\Sigma}^- \rightarrow \bar{p}\pi^0$)	$\Lambda\Sigma^+\pi^-$ ($\Sigma^+ \rightarrow n\pi^+$)	$\Lambda\Sigma^+\pi^-$ ($\Sigma^+ \rightarrow p\pi^0$)	$\Lambda\Sigma^-\pi^+$ ($\Sigma^- \rightarrow n\pi^-$)
Track detection efficiency	8	8	8	8	8	8
Particle identification	1	1	1	1	1	1
Photon detection efficiency	–	–	2	–	2	–
Fitting of Σ mass	3.6	2.7	0.7	3.1	2.6	1.5
Kinematic fit	2.0	2.0	1.7	2.0	1.7	2.0
Intermediate excited states	2.3	0.1	5.1	1.0	2.2	1.4
$\mathcal{B}(\Lambda \rightarrow p\pi^-)$	0.78	0.78	0.78	0.78	0.78	0.78
$\mathcal{B}(\Sigma^+ \rightarrow n\pi^+ \text{ or } p\pi^0)$	0.005	0.62	0.58	0.62	0.58	0.005
$\pi^0 \rightarrow \gamma\gamma$	–	–	0.034	–	0.034	–
Number of $\psi(3686)$ events	0.81	0.81	0.81	0.81	0.81	0.81
Total	9.4	8.8	9.9	9.0	9.2	8.6

- (2010).
- [13] M. Ablikim *et al.* (BES Collaboration), Phys. Rev. Lett. **97**, 062001 (2006).
- [14] M. Ablikim *et al.* (BES Collaboration), Phys. Rev. D **80**, 052004 (2009).
- [15] M. Ablikim *et al.* (BESIII Collaboration), Phys. Rev. Lett. **110**, 022001 (2013).
- [16] J. P. Alexander *et al.* (CLEO Collaboration), Phys. Rev. D **82**, 092002 (2010).
- [17] M. Ablikim *et al.* (BESIII Collaboration), Nucl. Instrum. Meth. A **614**, 345 (2010).
- [18] S. Agostinelli *et al.* (GEANT4 Collaboration), Nucl. Instrum. Meth. A **506**, 250 (2003).
- [19] Z. Y. Deng *et al.*, Chin. Phys. C **30**, 371 (2006).
- [20] S. Jadach, B. F. L. Ward and Z. Was, Comp. Phys. Commu. **130**, 260 (2000).
- [21] S. Jadach, B. F. L. Ward and Z. Was, Phys. Rev. D **63**, 113009 (2001).
- [22] R. G. Ping *et al.*, Chin. Phys. C **32**, 599 (2008).
- [23] J. C. Chen *et al.*, Phys. Rev. D **62**, 034003 (2000).
- [24] M. Ablikim *et al.* (BESIII Collaboration), arXiv:1307.2022.
- [25] M. Ablikim *et al.* (BESIII Collaboration), Chin. Phys. C **37**, 063001 (2013), arXiv:1209.6199.
- [26] M. Ablikim *et al.* (BESIII Collaboration), Phys. Rev. D **83**, 112005 (2011).
- [27] G. D'Agostini, Nucl. Instrum. Meth. A **346**, 306 (1994).